Progress In Electromagnetics Research, Vol. 134, 209–226, 2013

SAR IMAGE DESPECKLING BY SELECTIVE 3D FILTERING OF MULTIPLE COMPRESSIVE RECONSTRUCTED IMAGES

Mahboob Iqbal, Jie Chen*, Wei Yang, Pengbo Wang, and Bing Sun

School of Electronics and Information Engineering, Beihang University, Beijing 100191, China

Abstract—A despeckling technique based on multiple image reconstruction and selective 3-dimensional filtering is proposed. Multiple SAR images are reconstructed from a single SAR image by employing compressive sensing (CS) theory. In order to obtain multiple images from single SAR image, multiple subsets of pixels are selected from input SAR image by imposing restriction that each subset has at least 20% different pixels from any other subset. These subsets are taken as measurement vectors in CS framework to obtain multiple SAR images. A despeckled image is obtained by employing selective 3-dimensional filtering to multiple reconstructed SAR image. The proposed technique is tested on single look complex TerraSAT-X data set, and experimental results exhibit that the proposed technique outperformed benchmark despekling methods in terms of visual quality and despeckling quality metrics.

1. INTRODUCTION

Synthetic aperture radar (SAR) system is all-time and all-weather imaging system used for earth surveying. SAR systems transmit electromagnetic waves, and produce images by coherent integration of received pulses. In coherent systems, backscatter signals add to each other coherently, and random interference of electromagnetic signals causes the speckle noise [1]. Speckling is multiplicative noise which deteriorates the image quality. Recently, SAR systems have employed for several remote sensing applications such as environmental monitoring [2], surveillance [3, 4], target

Received 15 September 2012, Accepted 5 November 2012, Scheduled 24 November 2012
* Corresponding author: Jie Chen (chenjie@buaa.edu.cn).

identification [5], navigation [6], homeland security [7, 8] and target recognition [9]. The speckle noise in SAR images reduces the potential of SAR images to be utilized as effective data in remote sensing applications [10]. Therefore, despeckling (removal of speckle noise) is one of the more important tasks in SAR imaging.

The despeckling of SAR image has been a hot research area during last two decades. Classical despeckling methods such Lee [11], Frost [12] and Gamma-MAP [13] use a priori statistical information of speckle noise. These filters may over-smooth the textures. With the development of multi-resolution analysis theory, wavelet transformation methods are often used for despeckling [14, 15]. In Wavelet shrinkage techniques, wavelet transform coefficients are thresholded. The texture preservation in multi-resolution techniques is better compared to statistical techniques such as [11] and Frost [12], but performance of wavelet shrinkage techniques are quite sensitive to threshold limit. Non-local mean (NLM) approach has also been applied for despeckling of SAR images [16, 17]. NLM approaches are based on the observation that most images are comprised of self-similar patches. After identifying the self-similar patches, noise filtering is carried out in those patches. Block matching 3D (BM3D) [18] combines NLM and wavelet shrinkage. In BM3D, wavelet shrinkage is followed by collection of group of similar patches. In probabilistic patch based (PPB) algorihtm [19], a similarity criterion based on noise distribution method is considered and filtering weights are obtained through an iteration process which takes into account the similarity between restored patches.

The compressive sensing (CS) theory [20] proved that any sparse signal or image can be reconstructed from samples fewer than number of elements in a signal or image. Recently, CS theory has been used in SAR signal processing and image formation [21–24]. In this paper, we exploit CS theory for despeckling of SAR image. It is a well-known fact that multiple noisy images can be combined statistically to obtain cleaner image. Taking motivation from this phenomenon, we employ CS to obtain multiple SAR images from a single SAR image. A number of subsets of pixels are selected from input SAR image by imposing restriction that each subset has at least 20% different pixels than any other subset. These subsets are taken as measurement vectors in CS framework to obtain multiple SAR images by solving convex optimization problem. The pixel-wise averaging of multiple compressive reconstructed images would lead to better results compared to conventional despeckling techniques [25]. In this work, employ selective 3 dimensional (3D) filtering of multiple reconstructed images to further improve despeckling results. The

experimental results on single look SAR data set exhibited that the proposed technique outperformed benchmark as well as recent despeckling techniques in terms of qualitative and quantitative results.

The rest of the paper is organized as follows. A brief introduction of compressive sensing is given in Section 3. The proposed despeckling framework is described in Section 3 and experimental results are given in Section 4. Finally we conclude this paper in Section 5.

2. COMPRESSIVE SENSING FRAMEWORK

CS theory proved that a signal, which is sparse in some basis can be reconstructed from incomplete information, i.e., number of samples or measurements is less than the number of elements in the signal. Let $\mathbf{x}$ be an $N \times 1$ signal which is sparse in an orthonormal basis $\mathbf{\Psi} = [\psi_1, \psi_2, \ldots, \psi_{\mathbf{N}}]$. If M ($\ll N$) number of samples are acquired from signal by using $M \times N$ sampling matrix $\mathbf{S}$, the resulting vector (containing samples) can be written as [20]

$$\mathbf{y} = \mathbf{S}\mathbf{x} \tag{1}$$

The representation of $\mathbf{x}$ in sparse domain $\mathbf{\Psi}$ can be given as

$$\mathbf{x}^w = \mathbf{\Psi}\mathbf{x} \tag{2}$$

where $\mathbf{x}^w$ is $N \times 1$ vector with K ($K < M$) non-zero entries and $\mathbf{\Psi}$ is $N \times N$ sparse basis matrix. Using (2), the measurement vector can be written as

$$\mathbf{y} = \mathbf{S}\mathbf{\Psi}^{-1}\mathbf{x}^w \tag{3}$$

where $\mathbf{\Theta} = \mathbf{S}\mathbf{\Psi}^{-1}$ is an $M \times N$ matrix called measurement matrix. The problem of finding $\mathbf{x}^w$ from $\mathbf{y}$ is highly under-determined, as number of unknown N, is higher than the number of equations which is equal to M ($\ll N$). But if measurement matrix, $\mathbf{\Theta}$ satisfies Restricted Isometery Property (RIP), (3) can be solved by emplying efficient reconstruction techniques. RIP states for any vector ν sharing the same K non-zero entries as $\mathbf{v}$ and for some $\epsilon > 0$ [20]

$$1 - \epsilon \leq \frac{\|\mathbf{\Theta}\mathbf{v}\|^2}{\|\mathbf{v}\|^2} \leq 1 + \epsilon \tag{4}$$

If (4) is satisfied, signal $\mathbf{x}^w$ can be reconstructed from (3) by solving following l_1 optimization problem [20]

$$\hat{\mathbf{x}}^w = \min \|\mathbf{x}^w\|_1 \qquad \text{subject to} \qquad \mathbf{y} = \mathbf{\Theta}\mathbf{x}^w \tag{5}$$

(5) can be solved by employing a convex optimization algorithm, such as gradient point sparse reconstruction (GPSR) [26] or regularized orthogonal matching pursuit (ROMP) [27]. The convex optimization

algorithm requires $\mathbf{y} \in \mathbf{R}^M$ and measurement matrix, $\mathbf{\Theta} = \mathbf{S}\mathbf{\Psi}^{-1}$ to reconstruct $\hat{\mathbf{x}}^w \in \mathbf{R}^N$. The $\mathbf{x}$ is obtained by taking inverse $\mathbf{\Psi}$ transform of $\hat{\mathbf{x}}^w$.

Conventional CS sampling matrices takes information from several randomly selected sensors in one measurement [28]. In this proposed despeckling framework, this conventional CS sampling matrix cannot be used, as the proposed despeckling technique is aimed at reconstructing multiple SAR images using different subsets of pixels from SAR image. The point sampling matrix proposed by Sen and Darabi [29] collects information from one pixel in one sample. A subset of M pixels selected from original SAR image can be arranged as $M \times 1$ vector $\mathbf{y}$ to serve as input for (5). The $M \times N$ sampling matrix corresponding to $\mathbf{y}$ will be comprised of only one '1' in each row corresponding to locations of selected pixels within SAR image.

3. PROPOSED DESPECKLING TECHNIQUE

The proposed despeckling framework is comprised of three major steps; selection of subsets of pixels from SAR images, reconstruction of SAR image from each subset of pixels using CS theory, and statistical combining of multiple reconstructed images by employing selective 3D filtering. The proposed framework is shown in Fig. 1. The hierarchical steps of the proposed framework are described in detail in following subsections.

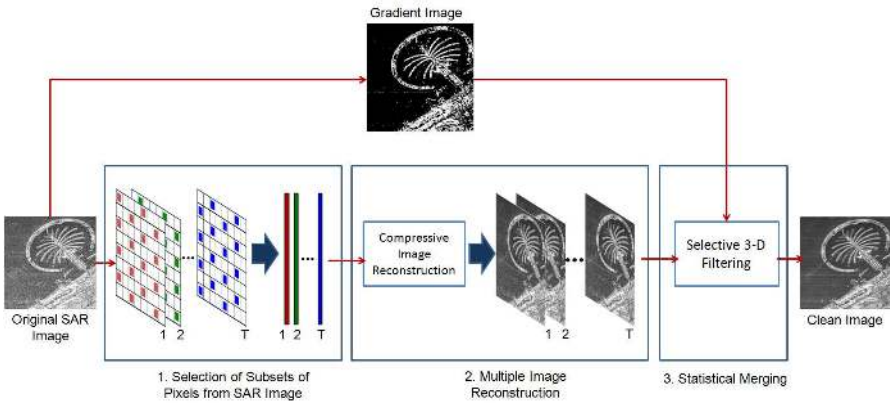

Figure 1. Proposed despeckling framework.

3.1. Selection of Multiple Subsets

In order to formulate multiple partially overlapped subsets of pixels from $m \times n$ SAR image, $\mathbf{x}$, first of all SAR image is divided into P mutually exclusive (ME) groups of pixels. The pixels in each group follow regular pattern, and pixels of same group are separated by fixed distance in horizontal and vertical directions as shown in Fig. 2. In Fig. 2, the pixels belonging to each group is represented by a unique symbol. These groups do not overlap and each group contains distinct pixels. The distance between pixels of same group in horizontal and vertical directions are h and v respectively. In Fig. 2, h is 4, v is 2 and $P = h \times v = 8$. Each group contains $S = N/P$ (where $N = m \cdot n$) pixels. If image is divided into more number of groups, the distances between pixels of same groups increases and vice versa.

Let p-th group of pixels be $\mathbf{u}_p$ with $p = 1, 2, \ldots, P$. If pixels in $\mathbf{u}_p$ are selected in regular pattern as shown in Fig. 2, it can be gievn by following expression by taking leverage from Matlab syntax

$$\mathbf{u}_p = x(\alpha : v : m, \beta : h : n) \tag{6}$$

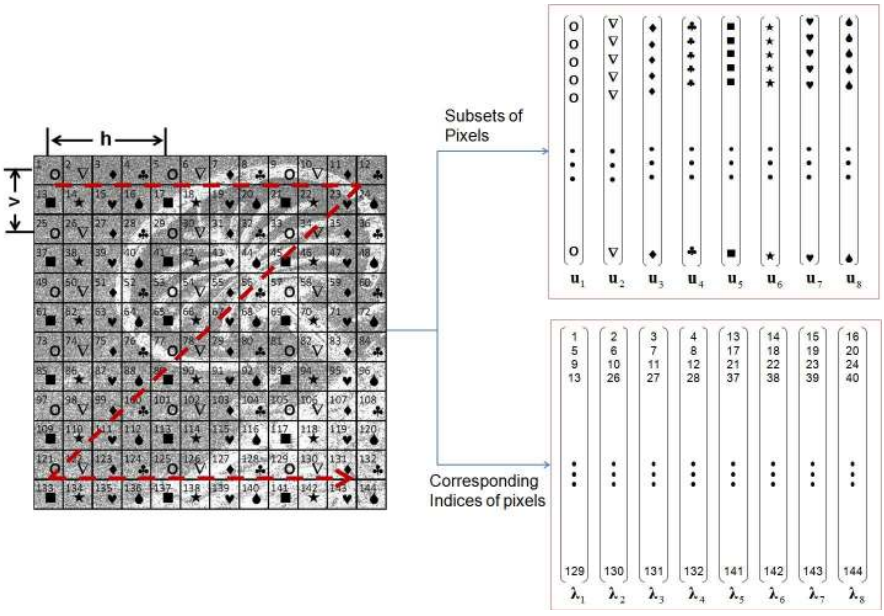

Figure 2. Selection of multiple mutually exclusive subsets of pixels. In this example, 8 subsets of pixels are selected from SAR image. Each group is represented by different symbol in the image. The corresponding indices of subsets are also shown as vectors.

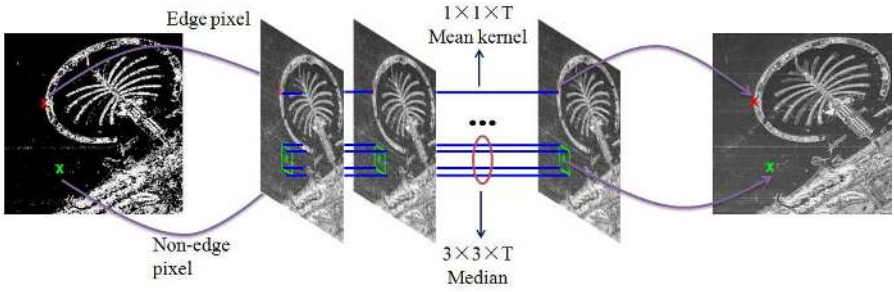

Figure 3. Three dimensional selective filtering.

where

$$\alpha = 1, 2, \ldots, v \quad \text{and} \quad \beta = 1, 2, \ldots, h$$

and

$$p = \beta + (\alpha - 1)h$$

with $p \in \{1, 2, \ldots, P\}$ and maximum value of $p = P\ (= v \cdot h)$ when $\alpha = v$ and $\beta = h$.

Similarly, vectors containing indices of pixels in original SAR image corresponding to $\mathbf{u}_p$ can be given as

$$\lambda_p = \{(i-1)n + j\}|_{\substack{i=\alpha:v:m \\ j=\beta:h:n}} \tag{7}$$

where p, α, β are same as for (6). An example of selection of $\mathbf{u}_p$ for Fig. 2 where, $h = 4$ and $v = 2$ is given as

$$\begin{aligned}
\mathbf{u}_1 &= \{x(i,j)|i = 1:2:m, j = 1:4:n\} \\
\mathbf{u}_2 &= \{x(i,j)|i = 1:2:m, j = 2:4:n\} \\
\mathbf{u}_3 &= \{x(i,j)|i = 1:2:m, j = 3:4:n\} \\
\mathbf{u}_4 &= \{x(i,j)|i = 1:2:m, j = 4:4:n\} \\
\mathbf{u}_5 &= \{x(i,j)|i = 2:2:m, j = 1:4:n\} \\
\mathbf{u}_6 &= \{x(i,j)|i = 2:2:m, j = 2:4:n\} \\
\mathbf{u}_7 &= \{x(i,j)|i = 2:2:m, j = 3:4:n\} \\
\mathbf{u}_8 &= \{x(i,j)|i = 2:2:m, j = 4:4:n\}
\end{aligned} \tag{8}$$

The multiple subsets of image pixels to be used as compressive samples for multiple reconstruction are formed by combining 'Q' number of ME groups of pixels selected from $\mathbf{U} = [\mathbf{u}_1, \mathbf{u}_2, \ldots, \mathbf{u}_P]$. The value of Q is selected based on tradeoff between number of multiple images and edge quality of reconstructed images. Lower value of Q means fewer pixels for reconstruction of image, hence results in poor

image quality of reconstructed images, but we can get higher number of reconstructed images. On the contrary, higher value of Q will produce sharp high quality reconstructed images, but the number of reconstructed images will be fewer. Experimental results show that 50% pixels would be able to produce sufficiently high quality sharp image, hence empirical value of $Q = P/2$. If Q number of ME groups of pixels are selected from P number of ME groups, total number of all possible subsets can be found by following expression

$$T = \binom{P}{Q} = \frac{P!}{Q!(P-Q)!} \tag{9}$$

where symbol '!' represents factorial. From (9), T distinct combinations of Q groups out P groups will be obtained. Let $\mathbf{C}_t = \{c_t^1, c_t^2, \ldots, c_t^Q\}$ be the t-th combination, where $\{c_t^1, c_t^2, \ldots, c_t^Q\}$ are non-repeating integers between 1 and T. For t-th distinct combination of Q groups of pixels out of P groups, subset $\mathbf{y}_t$ can be given as

$$\mathbf{y}_t = \bigcup (\mathbf{u}_c | c \in \mathbf{C}_t) \tag{10}$$

where $\mathbf{C}_t$ is a vector comprising of non-repeating integers between 1 and P. Similarly, vector comprising of indices of selected pixels corresponding to $\mathbf{y}_t$ is written as

$$\mathbf{\Lambda}_t = \bigcup (\lambda_c | c \in \mathbf{C}_t) \tag{11}$$

3.2. Multiple Compressive Image Reconstruction

Once multiple subsets of pixels have been selected from original SAR image, the next step is to reconstruct SAR image for each subset of pixels. The $\mathbf{y}_t$ is $M \times 1$ vector where $M = QS$. The SAR image can be reconstructed from each subset $\mathbf{y}_t$, $t \in \{1, T\}$ using CS theory described in Section 2 by considering $\mathbf{y}_t$ as compressive samples. The compressive sampling Equation (1) becomes

$$\mathbf{y}_t = \mathbf{S}_t \mathbf{x}_t = \mathbf{S}_t \mathbf{\Psi}^{-1} \hat{\mathbf{x}}_t^w = \mathbf{\Theta}_t \hat{\mathbf{x}}_t^w \tag{12}$$

where $\mathbf{\Theta}_t = \mathbf{S}_t \mathbf{\Psi}^{-1}$ is measurement matrix and $\hat{\mathbf{x}}_t^w$ a vector containing coefficients of $\hat{\mathbf{x}}_t$ in wavelet domain. In (12), $\mathbf{\Psi}^{-1}$ represent inverse wavelet transform. $\mathbf{S}_t$ is t-th sampling matrix corresponding to $\mathbf{y}_t$. It is $M \times N$ matrix produced by taking exactly one '1' in each of M rows corresponding to the location of pixel of $\mathbf{y}_t$ within SAR image. The sampling matrix for t-th subset is determined by using (11)

$$\mathbf{S}_t(\tau, \xi) = \begin{cases} 1 & \text{if } \Lambda(\tau) = \xi, \\ 0 & \text{otherwise.} \end{cases} \tag{13}$$

The point sampling matrix is not sufficiently incoherent with sparse basis [29], so a blurring filter is incorporated into measurement matrix as proposed by [29] and measurement matrix becomes

$$\mathbf{\Theta}_t = \mathbf{S}_t \mathbf{\Gamma}^{-1} \mathbf{\Psi}^{-1} \tag{14}$$

The blur introduced by blurring filter is removed by introducing a Weiner sharpening filter [30] in inverse measurement matrix [29]. The inverse measurement matrix is $\mathbf{\Theta}_t^* = \mathbf{\Psi}\mathbf{\Gamma}\mathbf{S}_t^{-1}$. A SAR image, $\mathbf{x}_t$ is reconstructed for each sampled vectors, $\mathbf{y}_t$ by solving following convex optimization problem

$$\min_{\hat{\mathbf{x}}_t^w \in \mathbf{R}^N} \|\hat{\mathbf{x}}_t^w\|_1 \qquad \text{subject to} \qquad \mathbf{y}_t = \mathbf{\Theta}_t \hat{\mathbf{x}}_t^w \tag{15}$$

(15) is solved for each $\mathbf{y}_t$ using gradient projection for sparse reconstruction (GPRS) [26] followed by inverse wavelet transform to obtain t-th image $\hat{\mathbf{x}}_t$.

T number of SAR images are reconstructed corresponding to T subsets by using (15). The speckle noise is located in high frequency component of image so sparse reconstruction of image would help eliminate noise in the reconstructed image. Therefore, all reconstructed images obtained by solving (15) have lower speckle noise compared to source image. In the final step, these multiple reconstructed images are statistically combined by employing selective 3D filtering as discussed in Section 3.3.

3.3. Selective 3-D Filtering

Multiple reconstructed images obtained using (15) are similar in global perspective but statistically different in local perspective as all these images are reconstructed by using different sets of pixels. It is well known that statistical processing of multiple observations of same scene help reduce additive and multiplicative noise. Moreover, spatial filtering such as low-pass filtering or median filtering also reduces noise. In order to exploit the availability of multiple images from single image, we propose a selective 3D filtering in this paper. In order to better preserve the edges in final despeckled image, the kernel for 3D filtering is selected as a function of image gradient.

To identify the presence of edges in an image, the image gradient is an important tool. The gradient of source SAR image $\mathbf{x}$ in horizontal and vertical directions can be given as

$$\mathbf{G}_h = \frac{\partial x}{\partial h} \approx \mathbf{f}_h * \mathbf{x} \quad \mathbf{G}_v = \frac{\partial x}{\partial v} \approx \mathbf{f}_v * \mathbf{x} \tag{16}$$

where '$*$' denotes 2 dimensional convolution; $\mathbf{G}_h$ and $\mathbf{G}_v$ are gradient approximations in horizontal and vertical directions respectively.

In (16), $\mathbf{f}_h$ and $\mathbf{f}_v$ are filter kernels in horizontal and vertical directions respectively given as follows

$$\mathbf{f}_h = \begin{pmatrix} -1 & 0 & +1 \\ -2 & 0 & +2 \\ -1 & 0 & +1 \end{pmatrix}, \quad \mathbf{f}_v = \begin{pmatrix} -1 & -2 & -1 \\ 0 & 0 & 0 \\ +1 & +2 & +1 \end{pmatrix} \tag{17}$$

The gradient approximations in horizontal and vertical directions can be combined to give the gradient magnitude, using

$$\mathbf{G} = \sqrt{\mathbf{G}_h^2 + \mathbf{G}_v^2} \tag{18}$$

$\mathbf{G}$ will have higher values at locations where edges are present and lower values in smoother areas. In the proposed technique, 3D filter is selected based on the value of gradient approximation at the central pixel location as shown in Fig. 3. If value of gradient approximation at any pixel $x(i,j)$ is less than $TH = \varrho \cdot G_{\max}$ (where $G_{\max}$ is maximum value at any pixel in $\mathbf{G}$ and ϱ is a positive constant), $R \times R$ window centered at subject pixel is selected for all T images, and median value of all selected pixels is returned as pixel at (i,j) location of despeckled SAR image. If gradient approximation is greater than the TH, the pixels at (i,j) location of all reconstructed images are averaged. In mathematical form, despeckled image, $\hat{\mathbf{x}}$ can be written as

$$\hat{x}(i,j) = \begin{cases} \text{MEDIAN}\left(\{x_t(k_1,k_2)\};\ \begin{matrix} t \in \{1,T\} \\ k_1 \in \{i-R, i+R\} \\ k_2 \in \{j-R, j+R\} \end{matrix}\right) & \text{if } G(i,j) < TH, \\ \frac{1}{T}\sum_{t=1}^{T} x_t(i,j) & \text{otherwise.} \end{cases} \tag{19}$$

where MEDIAN represents the median operation, T is the number of reconstructed images, and $2R+1$ is the size of selected window for each image. The image obtained by employing (19) is despeckled image. In the proposed framework speckle is reduced by imposing dual mechanisms; through inherent noise reduction via compressive reconstruction (15) and selective 3D filtering (19). Therefore, the proposed framework leads to better speckle reduction compared to benchmark despeckling algorithms.

4. IMPLEMENTATION AND EXPERIMENTAL RESULTS

4.1. Despeckled Image Quality Metrics

In order to measure the performance of despeckling techniques, following metrics are used.

4.1.1. ENL

Equivalent number of looks (ENL) [31] is one of the commonly used metric used to quantify the quality of despeckled SAR images. ENL is calculated by using following expression

$$ENL = \left(\frac{\mu_{\hat{\mathbf{x}}_H}}{\sigma_{\hat{\mathbf{x}}_H}}\right)^2 \tag{20}$$

where $\mu_{\hat{\mathbf{x}}_H}$ and $\sigma_{\hat{\mathbf{x}}_H}$ are mean and standard deviation of homogeneous area, $(\hat{\mathbf{x}}_H)$ in despeckled image. The higher the value of ENL, better the performance of despeckling technique.

4.1.2. Speckle Suppression Index

The ratio of standard deviation to mean (also called coefficient of variance) is used to measure the speckle strength in an image. Let $\mathbf{x}$ and $\hat{\mathbf{x}}$ be original and speckle reduced SAR images respectively. The speckle suppression index (SSI) is defined as the ratio of coefficient of variance of speckle resorter image to the coefficient of variance of original image as given below [32]

$$SSI = \frac{\sqrt{VAR(\hat{\mathbf{x}})}}{Mean(\hat{\mathbf{x}})}\frac{Mean(\mathbf{x})}{\sqrt{VAR(\mathbf{x})}} \tag{21}$$

SSI is less than 1. The smaller values of SSI means higher suppression of speckle noise [32].

4.1.3. Speckle Suppression and Mean Preservation Index

ENL and SSI are not considered as reliable measures when the despeckling algorithm overestimates the mean value. Therefore, speckle suppression and mean preservation index (SMPI) is used for simultaneous estimation of speckle suppression and mean preservation capabilities of despeckling technique. SMPI is given as [33]

$$SMPI = Q \times \frac{\sqrt{VAR(\hat{\mathbf{x}})}}{\sqrt{VAR(\mathbf{x})}} \tag{22}$$

where

$$Q = K + |Mean(\hat{\mathbf{x}}) - Mean(\mathbf{x})|$$

and

$$K = \frac{\max(Mean(\hat{\mathbf{x}})) - \min(Mean(\hat{\mathbf{x}}))}{Mean(\mathbf{x})}$$

4.1.4. Correlation Coefficient

The correlation coefficient (CC) for original image, $\mathbf{x}$, and despeckled image $\hat{\mathbf{x}}$ is calculated as follows

$$\rho_{x,\hat{x}} = \frac{E[(x-\mu_x)(\hat{x}-\mu_{\hat{x}})]}{\sigma_x \sigma_{\hat{x}}} \tag{23}$$

where μ_x and $\mu_{\hat{x}}$ are mean values of original and despeckled SAR images respectively and σ_x and $\sigma_{\hat{x}}$ are standard deviations of original and despeckled images respectively.

4.1.5. Edge Save Index

Edge save index (ESI) reflects the edge preservation capability of despeckling technique. ESI is measured in both horizontal and vertical directions. ESI in horizontal direction for $m \times n$ SAR image is computed as [34]

$$ESI^h = \frac{\sum_{i=1}^{m}\sum_{j=1}^{n-1}|\hat{x}(i,j+1)-\hat{x}(i,j)|}{\sum_{i=1}^{m}\sum_{j=1}^{n-1}|x(i,j+1)-x(i,j)|} \tag{24}$$

where $\hat{\mathbf{x}}$ is despeckled SAR image; $\mathbf{x}$ is original SAR image; m is the number of rows in SAR image; n is the number of columnsin SAR image. Similarly, ESI in vertical direction is given as

$$ESI^v = \frac{\sum_{j=1}^{n}\sum_{i=1}^{m-1}|\hat{x}(i+1,j)-\hat{x}(i,j)|}{\sum_{j=1}^{n}\sum_{i=1}^{m-1}|x(i+1,j)-x(i,j)|} \tag{25}$$

4.2. Experimental Results

The proposed despeckling technique was implemented in MATLAB and tested on TerraSAR-X [35] data set. In our implementation, we consider 8 non-overlapping subsets of pixels as shown in Fig. 2. For better preservation of edges, 50% pixels are used for reconstruction of image using GPSR algorithm [26]. In order to select 50% pixels, 4 subsets of pixels are selected out of 8 subsets leading to 70 sampling matrices. The obtained 70 images are combined by employing selective 3D filtering discussed in Section 3.3. The value of ρ to determine for threshold for (19) is taken as 0.01 to determine the value of TH in (19). Haar wavelets with decomposition level of 3 are used as sparse basis for solving (15).

The proposed despeckling technique is compared with benchmark and recent despeckling techniques such as Lee [11], Frost [36], Gamma-MAP [13], wavelets shrinkage [14], probabilistic patch based

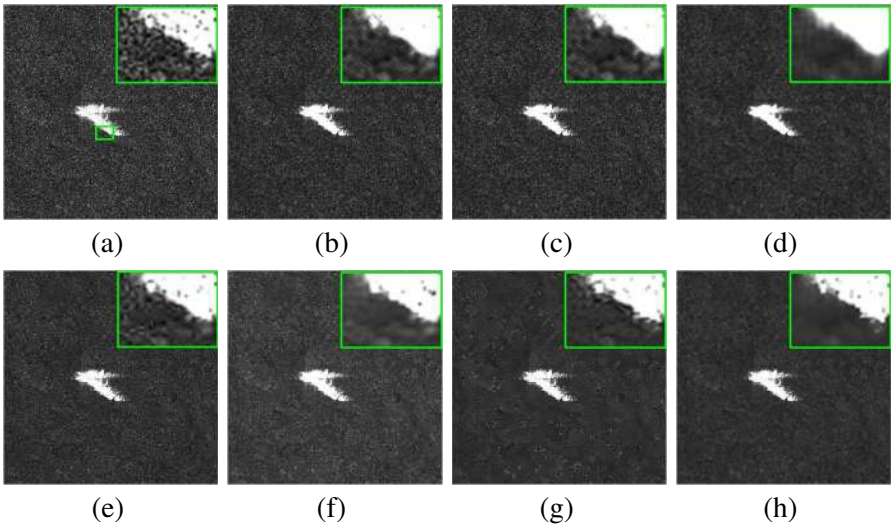

Figure 4. TerraSAR-X dataset: ship in sea. (a) Original (single look), (b) Lee, (c) Frost, (d) Gamma-MAP, (e) wavelet shrinkage [14], (f) BM3D [18], (g) PPB [19], (h) proposed.

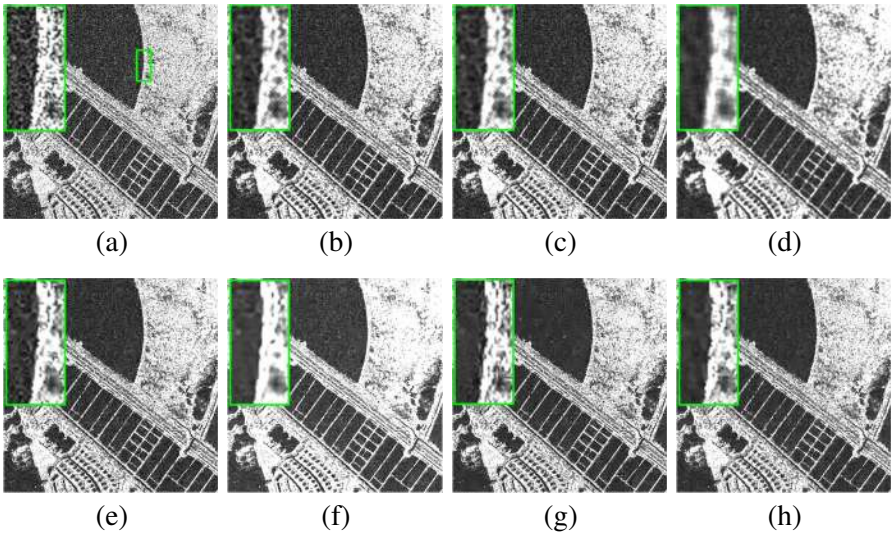

Figure 5. TerraSAR-X dataset: urban area of Tianjin, China. (a) Original (single look), (b) Lee, (c) Frost, (d) Gamma-MAP, (e) wavelet shrinkage [14], (f) BM3D [18], (g) PPB [19], (h) proposed.

technique [19] and block matching 3D (BM3D) [18]. Three patches are selected from single look complex (SLC) data of TerraSAR-X. The test TerraSAR-x images includes; ship in sea near Dubai coastal area, and urban/rural areas of Tianjin province, China. The despeckling results of the proposed technique and comparison methods for these three real SAR images are given in Fig. 4 to Fig. 6.

The experimental results shown in Fig. 4 to Fig. 6 exhibit that proposed despeckling technique performs better than classical despeckling filters and recent techniques in terms of visual quality. The proposed technique not only produces smoother images in homogenous areas but also preserve edges. The Gamma-MAP and wavelet shrinkage Techniques tend to blur edges while removing the speckle noise. On the other hand, BM3D [18] and PPB [19] preserve edges better compared to conventional despeckling techniques, but artifacts can be seen in the despeckled real SAR images as shown in Fig. 4 and Fig. 6. The proposed technique outperformed conventional despeckling techniques as well as BM3D and PPB in terms of edge preservation as well as undesired artifacts.

In order to quantify the performance of despeckling techniques, despeckling performance measuring metrics discussed in Section 4.1 are used. The quantitative results for Fig. 4 to Fig. 6 are given in

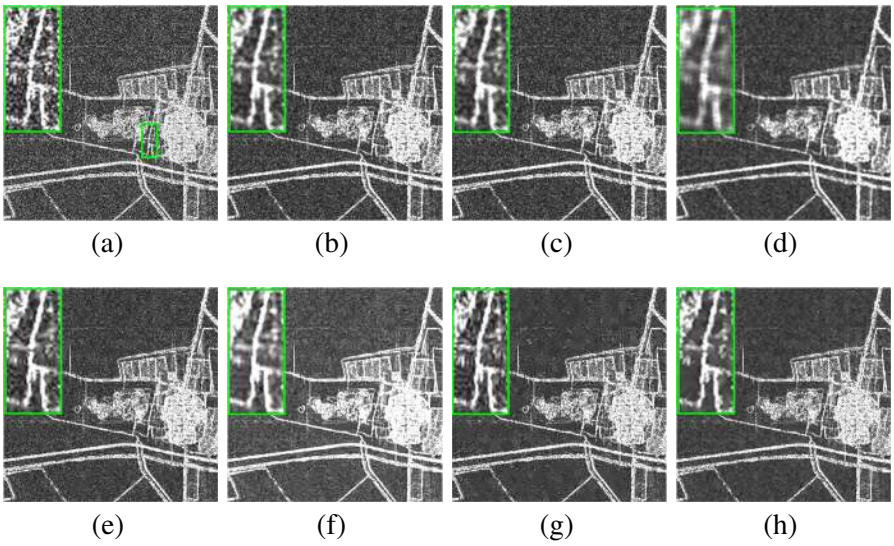

Figure 6. TerraSAR-X dataset: rural area of Tianjin, China. (a) Original (single look), (b) Lee, (c) Frost, (d) Gamma-MAP, (e) wavelet shrinkage [14], (f) BM3D [18], (g) PPB [19], (h) proposed.

Table 1. Quantitative comparison of despeckling techniques.

Metric	Best	Lee	Frost	Gamma -MAP	Wavelet	BM3D [18]	PPB [19]	Proposed
				Fig. 4				
ENL	↑	12.05	8.94	28.33	14.38	25.49	21.25	**35.13**
SSI	↓	0.1529	0.1773	0.0997	0.1399	0.1051	0.1164	**0.0783**
SMPI	↓	2.6120	2.7755	1.8968	2.124	1.9801	2.0141	**1.3789**
CC	↑	0.9019	0.9145	0.7245	0.9337	0.95087	0.9278	**0.9638**
ESI^h	↑	0.3183	0.4251	0.4345	0.4201	0.6008	0.6321	**0.6774**
ESI^v	↑	0.3095	0.4031	0.4708	0.4142	0.6059	0.6086	**0.6583**
				Fig. 5				
ENL	↑	11.29	8.58	27.19	15.75	26.22	26.24	**44.96**
SSI	↓	0.1505	0.1791	0.1006	0.1445	0.1028	0.1037	**0.0731**
SMPI	↓	3.6565	3.8133	2.6795	3.4075	2.8015	1.217	**0.9639**
CC	↑	0.9434	0.8969	0.7345	0.8941	0.9245	0.9296	**0.9450**
ESI^h	↑	0.3345	0.4284	0.3856	0.4627	0.4981	0.6714	**0.7183**
ESI^v	↑	0.3856	0.4517	0.3945	0.4624	0.4768	0.6287	**0.6714**
				Fig. 6				
ENL	↑	10.98	8.33	25.94	17.29	25.31	24.44	**41.71**
SSI	↓	0.1607	0.1839	0.1046	0.1484	0.1094	0.1064	**0.0874**
SMPI	↓	2.4832	2.608	1.8168	1.829	1.1986	1.5202	**1.1077**
CC	↑	0.9038	0.9239	0.7187	0.9184	0.9091	0.9367	**0.9387**
ESI^h	↑	0.3545	0.4514	0.3541	0.4571	0.4911	**0.7014**	**0.6974**
ESI^v	↑	0.3821	0.4718	0.3745	0.4401	0.4475	0.6314	**0.6438**

Table 1. It can be observed that the proposed despeckling technique performs better than other methods in terms of ENL, SSI, SMPI, CC and ESI^v. PPB [19] performed better than the proposed technique only in terms of ESI^h for Fig. 6, but the its performance is worse than the proposed method in terms of all other metrics for all three test images. Moreover, it can be seen that speckle suppression capability of PPB [18] is poor compared to the proposed methods as given in Table 1. Overall, the proposed despeckling techniques outperformed benchmark and recent despeckling techniques.

5. CONCLUSION

A SAR despeckling technique has been proposed using multiple compressive reconstructed images and selective 3D filtering. Multiple SAR images are obtained from single SAR image by using compressive sensing framework. The multiple SAR images are reconstructed in sparse domain by considering partially overlapped subsets of pixels as compressive samples, and employing convex optimization algorithm. The proposed scheme enforces two-fold noise-removal mechanism; noise elimination while reconstruction of image in sparse domain and statistical combining of multiple reconstructed images through 3D filtering. The experimental results on single look TerraSAR-x data set demonstrated the superiority of the proposed technique over benchmark despeckling techniques in terms of visual quality as well as despeckling image quality metrics.

ACKNOWLEDGMENT

This work is supported in part by the National Key Basic Research Program Project (973 Program) under Grant 2010CB731902, and in part by National Natural Science Foundation of China under Grant No. 61132006.

REFERENCES

1. Saevarsson, B. B., J. R. Sveinsson, and J. A. Benediktsson, "Combined wavelet and curvelet denoising of SAR images," *Geoscience and Remote Sensing Symposium, 2004 IEEE International Proceedings, IGARSS'04*, Vol. 6, 4235–4238, Sept. 2004.
2. Koo, V. C., Y. K. Chan, V. Gobi, M. Y. Chua, C. H. Lim, C.-S. Lim, C. C. Thum, T. S. Lim, Z. Bin Ahmad, K. A. Mahmood, M. H. Bin Shahid, C. Y. Ang, W. Q. Tan, P. N. Tan, K. S. Yee, W. G. Cheaw, H. S. Boey, A. L. Choo, and B. C. Sew, "A new unmanned aerial vehicle synthetic aperture radar for environmental monitoring," *Progress In Electromagnetics Research*, Vol. 122, 245–268, 2012.
3. Mohammadpoor, M., R. S. A. Raja Abdullah, A. Ismail, and A. F. Abas, "A circular synthetic aperture radar for on-the-ground object detection," *Progress In Electromagnetics Research*, Vol. 122, 269–292, 2012.
4. Brusch, S., S. Lehner, T. Fritz, M. Soccorsi, A. Soloviev, and B. van Schie, "Ship surveillance with TerraSAR-X," *IEEE*

Transactions on Geoscience and Remote Sensing, Vol. 49, No. 3, 1092–1103, Mar. 2011.

5. Park, J.-I. and K.-T. Kim, "A comparative study on isar imaging algorithms for radar target identification," *Progress In Electromagnetics Research*, Vol. 108, 155–175, 2010.
6. Ren, S., W. Chang, T. Jin, and Z. Wang, "Automated SAR reference image preparation for navigation," *Progress In Electromagnetics Research*, Vol. 121, 535–555, 2011.
7. Eineder, M., C. Minet, P. Steigenberger, X. Cong, and T. Fritz, "Imaging geodesy-toward centimeter-level ranging accuracy with TerraSAR-X," *IEEE Transactions on Geoscience and Remote Sensing*, Vol. 49, No. 2, 661–671, Feb. 2011.
8. Martnez-Lorenzo, J. A., F. Quivira, and C. M. Rappaport, "SAR imaging of suicide bombers wearing concealed explosive threats," *Progress In Electromagnetics Research*, Vol. 125, 255–172, 2012.
9. Chang, Y.-L., C.-Y. Chiang, and K.-S. Chen, "SAR IMA simulation with application to target recognition," *Progress In Electromagnetics Research*, Vol. 119, 35–57, 2011.
10. Lee, J.-S. and E. Pottier, *Polarimetric Radar Imaging from Basics to Applications*, CRC Press, 2009.
11. Lee, J. S., L. Jurkevich, P. Dewaele, P. Wambacq, and A. Oosterlinck, "Speckle filtering of synthetic aperture radar images: A review," *Remote Sensing Reviews*, Vol. 8, No. 4, 313–340, 1994.
12. Frost, V. S., J. A. Stiles, K. S. Shanmugan, and J. C. Holtzman, "A model for radar images and its application to adaptive digital filtering of multiplicative noise," *IEEE Transactions on Pattern Analysis and Machine Intelligence*, Vol. 4, No. 2, 157–166, Mar. 1982.
13. Baraldi, A. and F. Parmiggiani, "A refined gamma map SAR speckle filter with improved geometrical adaptivity," *IEEE Transactions on Geoscience and Remote Sensing*, Vol. 33, No. 5, 1245–1257, Sept. 1995.
14. Dai, M., C. Peng, A. K. Chan, and D. Loguinov, "Bayesian wavelet shrinkage with edge detection for SAR image despeckling," *IEEE Transactions on Geoscience and Remote Sensing*, Vol. 42, No. 8, 1642–1648, Aug. 2004.
15. Gleich, D., M. Kseneman, and M. Datcu, "Despeckling of terrasar-x data using second-generation wavelets," *IEEE Geoscience and Remote Sensing Letters*, Vol. 7, No. 1, 68–72, Jan. 2010.
16. Xu, J., H. Zhong, and L. Jiao, "Classification based non-

local means despeckling for SAR image," *Proceedings of SPIE*, Vol. 7495, 2009.

17. Coupe, P., P. Hellier, C. Kervrann, and C. Barillot, "Bayesian non local means-based speckle filtering," *5th IEEE International Symposium on Biomedical Imaging: From Nano to Macro, ISBI 2008*, 1291–1294, May 2008.
18. Parrilli, S., M. Poderico, C. V. Angelino, and L. Verdoliva, "A nonlocal SAR image denoising algorithm based on llmmse wavelet shrinkage," *IEEE Transactions on Geoscience and Remote Sensing*, Vol. 50, No. 2, 606–616, Feb. 2012.
19. Deledalle, C.-A., L. Denis, and F. Tupin, "Iterative weighted maximum likelihood denoising with probabilistic patch-based weights," *IEEE Transactions on Image Processing*, Vol. 18, No. 12, 2661–2672, Dec. 2009.
20. Donoho, D. L., "Compressed sensing," *IEEE Transactions on Information Theory*, Vol. 52, No. 4, 1289–1306, Apr. 2006.
21. Chen, J., J. Gao, Y. Zhu, W. Yang, and P. Wang, "A novel image formation algorithm for high-resolution wide-swath spaceborne SAR using compressed sensing on azimuth displacement phase center antenna," *Progress In Electromagnetics Research*, Vol. 125, 527–543, 2012.
22. Wei, S.-J., X.-L. Zhang, and J. Shi, "Linear array SAR imaging via compressed sensing," *Progress In Electromagnetics Research*, Vol. 117, 299–319, 2011.
23. Li, J., S. Zhang, and J. Chang, "Applications of compressed sensing for multiple transmitters multiple azimuth beams SAR imaging," *Progress In Electromagnetics Research*, Vol. 127, 259–275, 2012.
24. Xing, S., D. Dai, Y. Li, and X. Wang, "Polarimetric SAR tomography using $\ell_{2,1}$ mixed norm sparse reconstruction method," *Progress In Electromagnetics Research*, Vol. 130, 105–130, 2012.
25. Iqbal, M. and J. Chen, "Despecking of SAR images using compressive imaging framework," *Geoscience and Remote Sensing Symposium, 2012 IEEE International Proceedings, IGARSS'12*, 264–267, Jul. 2012.
26. Figueiredo, M. A. T., R. D. Nowak, and S. J. Wright, "Gradient projection for sparse reconstruction: Application to compressed sensing and other inverse problems," *IEEE Journal of Selected Topics in Signal Processing*, Vol. 1, No. 4, 586–597, Dec. 2007.
27. Needell, D. and R. Vershynin, "Signal recovery from incomplete and inaccurate measurements via regularized orthogonal matching

pursuit," *IEEE Journal of Selected Topics in Signal Processing*, Vol. 4, No. 2, 310–316, Apr. 2010.

28. Wakin, M. B., J. N. Laska, M. F. Duarte, D. Baron, S. Sarvotham, D. Takhar, K. F. Kelly, and R. G. Baraniuk, "An architecture for compressive imaging," *2006 IEEE International Conference on Image Processing*, 1273–1276, Oct. 2006.
29. Sen, P. and S. Darabi, "Compressive rendering: A rendering application of compressed sensing," *IEEE Transactions on Visualization and Computer Graphics*, Vol. 17, No. 4, 487–499, Apr. 2011.
30. Gonzalez, R. C. and R. E. Woods, *Digital Image Processing*, Prentice Hall, New York, 2008.
31. Gagnon, L. and A. Jouan, "Speckle filtering of SAR images: A comparative study between complex-wavelet-based and standard filters," *Proceedings of SPIE*, Vol. 3169, 1997.
32. Shen, Y. and Z.-G. Xia, "A comprehensive evaluation of filters for radar speckle suppression," *Geoscience and Remote Sensing Symposium, 1996 IEEE International Proceedings, IGARSS'96*, Vol. 3, 1559–1561, May 1996.
33. Shamsoddini, A. and J. C. Trinder, "Image texture preservation in speckle noise suppression," *ISPRS TC VII Symposium — 100 Years ISPR*, W. Wagner and B. Szkely (eds.), Vol. XXXVIII, Part 7A, 239–244, Vienna, Austria, Jul. 5–7, 2010.
34. Zhang, W., F. Liu, L. Jiao, B. Hou, S. Wang, and R. Shang, "SAR image despeckling using edge detection and feature clustering in bandelet domain," *IEEE Geoscience and Remote Sensing Letters*, Vol. 7, No. 1, 131–135, Jan. 2010.
35. Breit, H., T. Fritz, U. Balss, M. Lachaise, A. Niedermeier, and M. Vonavka, "Terrasar-x SAR processing and products," *IEEE Transactions on Geoscience and Remote Sensing*, Vol. 48, No. 2, 727–740, Feb. 2010.
36. Frost, V. S., J. A. Stiles, K. S. Shanmugan, and J. C. Holtzman, "A model for radar images and its application to adaptive digital filtering of multiplicative noise," *IEEE Transactions on Pattern Analysis and Machine Intelligence*, Vol. 4, No. 2, 157–166, Mar. 1982.